

Emerging spatial curvature can resolve the tension between high-redshift CMB and low-redshift distance ladder measurements of the Hubble constant

Krzysztof Bolejko

*Sydney Institute for Astronomy, School of Physics,
A28, The University of Sydney, NSW, 2006, Australia*

The measurements of the Hubble constant reveal a tension between high-redshift (CMB) and low-redshift (distance ladder) constraints. So far neither observational systematics nor new physics has been successfully implemented to explain this tension away. This paper presents a new solution to the Hubble constant problem. The solution is based on the Simsilun simulation (relativistic simulation of the large scale structure of the Universe) with the ray-tracing algorithm implemented. The initial conditions for the Simsilun simulation were set up as perturbations around the Λ CDM model. However, unlike in the Standard Cosmological Model (i.e. Λ CDM model + perturbations), within the Simsilun simulation relativistic and nonlinear evolution of cosmic structures leads to the phenomenon of emerging spatial curvature, where the mean spatial curvature evolves from spatial flatness of the early universe towards slightly curved present-day universe. Consequently, the present-day expansion rate is slightly faster compared to the spatially flat Λ CDM model. The results of the ray-tracing analysis show that the universe which starts with initial conditions consistent with the Planck constraints should have the Hubble constant $H_0 = 72.5 \pm 2.1 \text{ km s}^{-1} \text{ Mpc}^{-1}$. When the Simsilun simulation was re-run with no inhomogeneities imposed, the Hubble constant inferred within such a homogeneous simulation was $H_0 = 68.1 \pm 2.0 \text{ km s}^{-1} \text{ Mpc}^{-1}$. Thus, the inclusion of nonlinear relativistic evolution that leads to the emergence of the spatial curvature can explain why the low-redshift measurements favour higher values compared to high-redshift constraints and alleviate the tension between the CMB and distance ladder measurements of the Hubble constant.

PACS numbers: 98.80.-k, 98.80.Es, 98.80.Jk

I. INTRODUCTION

For the last 20 years, the Λ CDM model has been a successful concordance model. A single, spatially flat model was able to explain properties of high-redshift (early times) and low-redshift (late times) universe. However, with increasing precision of measurements and increasing amount of data, some tensions between various constraints start to appear [1]. While some of these tensions are subject to observational biases and systematics, which means they are likely to be resolved in the near future, some could pose challenges to the standard Λ CDM model and point towards various extensions of the standard cosmological model. One of the most well known example of such tensions is the tension in the measurements of the Hubble constant: low-redshift measurements of the Hubble constant point towards $H_0 = 73.24 \pm 1.74 \text{ km s}^{-1} \text{ Mpc}^{-1}$ [2] whereas the Hubble constant inferred from the CMB (high-redshift) is $H_0 = 67.81 \pm 0.92 \text{ km s}^{-1} \text{ Mpc}^{-1}$ [3].

This paper argues that the H_0 tension is a manifestation of rigidity of the FLRW geometry. Within the FLRW models, if the spatial curvature is flat (the case of the Λ CDM model), it remains flat and does not change with time. The spatial flatness of the early Universe is predicted by inflation [4] and seems to be confirmed by the CMB constraints [3]. Therefore, if our Universe is correctly described (from the early universe till the present day) by the FLRW geometry, then the spatial flatness of the early universe should be preserved. However, if the geometry of our Universe slightly deviates

from the FLRW geometry (for example due to the evolution of cosmic structures [5]), then the spatial curvature will not be constrained and spatial flatness may not be preserved [6, 7]. Direct measurements of the spatial curvature using the low-redshift data (as opposed to fitting the FLRW model to the data) do not place tight constraints on the spatial curvature and allow for large range of possible values, including spatial flatness [8].

Understanding the phenomenon of the emerging spatial curvature requires fully relativistic cosmological simulations. However, such simulations are not easy, and so far have not been fully developed [9]. Cosmological relativistic simulations based on the Einstein toolkit [10], which implements the BSSN formalism [11–13] have difficulties with shell crossing singularities. Implementations of post-Newtonian corrections within N-body simulations, do not exhibit problems with shell crossings but face a problem of periodic boundary conditions, which impose a constraint on the global spatial curvature and force it to vanish [14]. This paper uses a relativistic simulation that is based on the approximation of the ‘Silent Universes’ – the Simsilun simulation [15]. The Simsilun simulation starts with perturbations around the Λ CDM model. These perturbations are allowed to have a non-zero spatial curvature. Initially, negative curvature of underdense regions is compensated by positive curvature of overdense regions. Once the evolution enters the non-linear regime, the symmetry between overdensities and underdensities is broken, consequently the mean spatial curvature of the universe slowly drifts from zero towards negative curvature induced by cosmic voids.

The results of the Simsilun simulation indicate that the present-day curvature of our universe is approximately $\Omega_k(z \approx 0) \sim 0.1$, as compared to spatial flatness of the early universe $\Omega_k(z \gg 0) = 0$.

This paper uses the Simsilun simulation (Sec. III) and implements the ray-tracing algorithm to generate mock data (Sec. IV). The analysis of the mock catalogues shows that the Hubble constant inferred from low-redshift data should in fact be higher compared to high-redshift constraints (Sec. V).

II. MEASUREMENTS OF THE HUBBLE CONSTANT

A. The method of inferring the Hubble constant from CMB

The Hubble constant inferred from the CMB is a highly model-dependent measurement of the present-day expansion rate H_0 [3]. The parameter H_0 is not measured directly but derived from other parameters. The standard practice is to fit 6 base parameters of the Λ CDM model and from them estimate H_0 . These six base parameters constitute: physical baryon density $\omega_b = \Omega_b h^2$, physical cold dark matter density $\omega_c = \Omega_c h^2$, optical depth τ , the amplitude of the dimensional, primordial curvature power spectrum A_s , and its spectral index n_s . The last 6th parameter is either the acoustic scale θ (Planck analysis, [3]) or the parameter Ω_Λ (WMAP analysis, [16]).

These two last parameters θ and Ω_Λ are not independent from each other. The acoustic scale is defined as a ratio of the sound horizon at decoupling r_s (which depends on physical matter density ω_b , ω_c , and radiation density ω_r) to the angular distance to the last scattering surface D_A (which depends on physical matter density ω_b , ω_c , radiation density ω_r , and dark energy density $\omega_\Lambda = \Omega_\Lambda h^2$). Since, radiation energy density is fixed by the CMB temperature it is not really a free parameter, so apart from ω_b and ω_c (which are already listed above) the only free parameter that θ depends on is ω_Λ .

The Hubble constant is then derived: from the dependence of the shape of the CMB power spectrum on $\Omega_m h^3$, and the relative height of the acoustic peaks that are sensitive to $\Omega_m h^2$ (Planck analysis, [3]):

$$H_0 = 100 \text{ km s}^{-1} \text{ Mpc}^{-1} \Omega_m h^3 / \Omega_m h^2,$$

or from the condition of the spatial flatness (WMAP analysis, [16]):

$$H_0 = 100 \text{ km s}^{-1} \text{ Mpc}^{-1} \sqrt{\omega_b + \omega_c + \omega_\Lambda}.$$

The physical justification of such a measurement is as follows: the CMB mostly constrains the physical conditions of the early universe, i.e. physical density of baryons, cold dark matter, and radiation. If one assumes that the evolution of the universe after the decoupling instant is correctly described by the FLRW model

then the physical density can be translated to the expansion rate of the present-day universe, H_0 . In order to distinguish this parameter from the direct measurement of the present-day expansion rate (i.e. low-redshift observations of the expansion rate) let us denote it by H_0^{CMB} . The value of the Hubble constant estimated based on measurements obtained by the satellite Planck is $H_0^{\text{CMB}} = 67.81 \pm 0.92 \text{ km s}^{-1} \text{ Mpc}^{-1}$ [3].

B. The method of inferring the Hubble constant from distance ladder

At low-redshifts the Taylor expanded FLRW luminosity distance-redshift relation is

$$D_L(z) = \frac{cz}{H_0} \left(1 + \frac{1}{2} [1 - q_0] z - \frac{1}{6} [1 - q_0 - 3q_0^2 + j_0] z^2 \right). \quad (1)$$

This low-redshift series is independent of the matter content of the universe, and the only free parameter apart from H_0 are q_0 and j_0 that can be fixed by the low-redshift data only. In Ref. [2] these parameters were set to $q_0 = -0.55$ and $j_0 = 1$ (any realistic variation in q_0 and j_0 has a minor dependence on the inferred value of H_0).

Using the distance modulus to replace the distance with absolute and apparent magnitudes m and M

$$m - M = 5 \log_{10} D_L + 25, \quad (2)$$

the Hubble constant can be written as [2]

$$\log_{10} H_0 = \frac{M + 5a + 25}{5}, \quad (3)$$

where

$$a = \log_{10} \left(cz \left\{ 1 + \frac{1}{2} [1 - q_0] z - \frac{1}{6} [1 - q_0 - 3q_0^2 + j_0] z^2 \right\} \right) - 0.2m. \quad (4)$$

Thus, to estimate the Hubble constant H_0 one needs: redshift z , apparent magnitude m , and the absolute magnitude M . While z and m are directly observable, the absolute magnitude M requires calibrations of standard (or standardisable) candles. The calibration can be done using the distance ladder, which uses objects at different distances to calibrate others. In order to distinguish the Hubble parameter derived using the distance ladder method (DL) let us denote it as H_0^{DL} . The inferred value of the Hubble constant based on low-redshift data is $H_0^{\text{DL}} = 73.24 \pm 1.74 \text{ km s}^{-1} \text{ Mpc}^{-1}$ [2].

As noted in Sec. II A, $H_0^{\text{CMB}} = 67.81 \pm 0.92 \text{ km s}^{-1} \text{ Mpc}^{-1}$ and so there is a tension between H_0^{DL} and H_0^{CMB} . In the next section it will be argued that the main difference between H_0^{DL} and H_0^{CMB} is not due to observational systematics. If the average spatial curvature of our universe evolves from spatial flatness to non-negligible negative values at the present day, then one should in fact expect a difference between H_0^{CMB} and H_0^{DL} .

III. MODELLING THE RELATIVISTIC EVOLUTION OF THE UNIVERSE

A. Silent Universes

The approximation of the Silent Universes is derived within the 1+3 split [17, 18]. Here, one first introduces the comoving gauge with the velocity field $u^a \sim \delta_0^a$, and assumes that the gravitational field is sourced by irrotational and insulated dust. Then applying the energy-momentum conservation $T^{ab}{}_{;b} = 0$, the Ricci identities $u_{a;d;c} - u_{a;c;d} = R_{abcd}u^b$, and the Bianchi identities $R_{ab[cd;e]} = 0$, and finally assuming with the magnetic part of the Weyl tensor vanish, one reduces the Einstein equations to only 4 equations, which describe the evolution of dust (with matter density ρ), its velocity field (with expansion rate Θ and shear Σ) and the Weyl curvature \mathcal{W} [19, 20]

$$\dot{\rho} = -\rho\Theta, \quad (5)$$

$$\dot{\Theta} = -\frac{1}{3}\Theta^2 - \frac{1}{2}\kappa\rho - 6\Sigma^2 + \Lambda, \quad (6)$$

$$\dot{\Sigma} = -\frac{2}{3}\Theta\Sigma + \Sigma^2 - \mathcal{W}, \quad (7)$$

$$\dot{\mathcal{W}} = -\Theta\mathcal{W} - \frac{1}{2}\kappa\rho\Sigma - 3\Sigma\mathcal{W}, \quad (8)$$

where $\kappa = 8\pi G/c^4$. In addition to these equations, the evolution of the volume V of the fluid's element is given by

$$\dot{V} = V\Theta. \quad (9)$$

Apart from the evolution equations there are also spatial constraints. However, if these constraints are initially satisfied, they will be preserved in the course of the evolution [20, 21]. Thus, once the initial conditions are properly set up, the evolution of a relativistic system can be evaluated based on the above equations only. Finally, there is also the ‘Hamiltonian’ constraint which can be used to evaluate the spatial curvature

$$\frac{1}{6}\mathcal{R} = \frac{1}{3}\kappa\rho + \Sigma^2 - \frac{1}{9}\Theta^2 + \frac{1}{3}\Lambda. \quad (10)$$

1. FLRW limit

In the limit of spatial homogeneity and isotropy the Silent Universes reduces to the FLRW models. The condition of spatial homogeneity and isotropy implies that shear vanishes at every point in space and time, hence $\Sigma \equiv 0 \equiv \dot{\Sigma}$, which also implies $\mathcal{W} = 0$ and $\dot{\mathcal{W}} = 0$. Thus, the last two equations of the Silent Universe are trivial. The condition of spatial homogeneity and isotropy also leads to $\Theta \rightarrow 3\dot{a}/a$, where the function $a(t)$ depends on time only and is the FLRW scale factor (thus the scalar of the expansion Θ is 3 times the Hubble parameter).

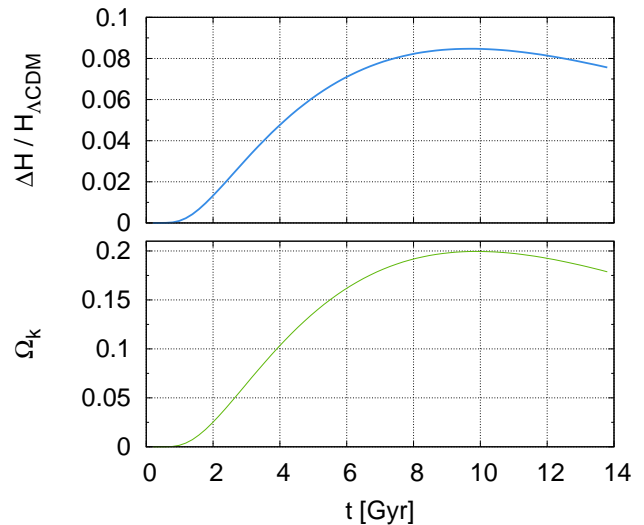


FIG. 1: Evolution of the global (mean) expansion rate (Upper panel) and the spatial curvature (Lower panel) within the Simsilun simulation. The initial conditions for the Simsilun simulation has been setup using density fluctuations from the Millennium simulation imposed on the Planck’s Λ CDM model at $z_i = 80$. As long as perturbations remain within the linear regime ($t < 1$ Gyr) the mean evolution follows the Λ CDM model. Once the system enters non-linear regime the spatial curvature emerges and the expansion rate slightly increases compared to the Λ CDM model.

Then the first equation of the Silent Universe reduces to $\rho = \rho_i a^{-3}$, and the second reduces to

$$3\frac{\ddot{a}}{a} = -\frac{1}{2}\kappa\rho + \Lambda, \quad (11)$$

which is the first Friedmann equation. In the limit of spatial homogeneity and isotropy, the spatial curvature reduces to $\mathcal{R} \rightarrow 6k/a^2$ and the Hamiltonian constraint becomes

$$3\frac{\dot{a}^2}{a^2} = \kappa\rho - 3\frac{k}{a^2} + \Lambda, \quad (12)$$

which is the first Friedmann equation.

B. Simsilun simulation

The evolutionary equations of the Silent Universe, i.e. (5)–(8) has been implemented in the code *simsilun* [49]. The description of the code, equations, and applications are described in the ‘Methods Paper’ [15]. The Methods Paper describes how one can use the Millennium simulation [22–24] to set up the initial condition for the code *simsilun*. The initial conditions are set up using the smoothed density field of the Millennium simulation stored in the MField database [50].

In this paper we apply a slight modification of the *Simsilun simulation* discussed in the Methods Paper [15]. The MField consists of 256^3 cells, that contain information about the matter density field smoothed with Gaussian kernel of radius $1.25 h^{-1}$ Mpc, $2.5 h^{-1}$ Mpc, $5 h^{-1}$ Mpc, and $10 h^{-1}$ Mpc. Unlike in the Methods Paper, where the smoothing scale was $2.5 h^{-1}$ Mpc, here we use the matter field smoothed with $1.25 h^{-1}$ Mpc radius, as it reproduces the parameter σ_8 more accurately — the smoothing decreases the variance of the density field so the larger the smoothing radius the smaller the parameter σ_8 : with $1.25 h^{-1}$ Mpc smoothing kernel the parameter σ_8 is underestimated by less than 2%, with $2.5 h^{-1}$ Mpc by 13%, $5 h^{-1}$ Mpc by 30%, and with $10 h^{-1}$ Mpc by almost 60%. The second change, compared to the Methods Paper is the change of the background cosmology. The *Simsilun* simulation described in the Methods Paper is based on the WMAP1 cosmology, just as the Millennium simulation. Here we assume that the background model is the Planck’s Λ CDM model, and we use it to set up the initial conditions for the *Simsilun* simulation. The initial background density $\bar{\rho}_i$ and the initial background’s expansion rate $\bar{\Theta}_i$ are

$$\begin{aligned}\bar{\rho}_i &= \Omega_m \frac{3H_0^2}{8\pi G} (1+z_i)^3 = \omega_m \frac{3}{8\pi G} (1+z_i)^3 H_{100}^2 \quad (13) \\ \bar{\Theta}_i &= 3 H_{100} \sqrt{\omega_m (1+z_i)^3 + \omega_\Lambda}, \quad (14)\end{aligned}$$

where $H_{100} = 100 \text{ km s}^{-1} \text{ Mpc}^{-1}$, $\omega_m = \Omega_m h^2 = 0.1415$, and $\omega_\Lambda = \Omega_\Lambda h^2 = 0.3182$ [3]. We then use the initial perturbations at $z_i = 80$, which follow from the Millennium’s snapshot no 1, and superimpose them onto the Planck’s Λ CMD background model ($\bar{\rho}_i$ and $\bar{\Theta}_i$). This serves as the initial conditions for our new simulation, that is based on evolving 16,777,216 worldlines (i.e. 256^3 cells) using eqs. (5)–(9) up to $z = 0$.

As discussed in the Methods Paper, the result of the evolution of the Silent Universe is emergence of the spatial curvature. The emergence of the spatial curvature is associated with the increase of the mean expansion rate, which is presented in Fig. 1. The mean expansion rate is defined as the volume average

$$H_{\mathcal{D}} = \frac{1}{3} \langle \Theta \rangle_{\mathcal{D}} = \frac{1}{3} \frac{\sum_n \Theta_n V_n}{\sum_n V_n}, \quad (15)$$

where the domain \mathcal{D} is the whole domain of the *Simsilun* simulation, Θ_n is the expansion rate of a single worldline/cell, and V_n is its volume, and $\sum_n V_n$ is volume of the entire domain of the *Simsilun* simulation. The parameter $\Omega_k^{\mathcal{D}}$ of the spatial curvature is

$$\Omega_k^{\mathcal{D}} = -\frac{\langle \mathcal{R} \rangle_{\mathcal{D}}}{6H_{\mathcal{D}}^2}. \quad (16)$$

In the limit of spatial homogeneity and isotropy, each cell has the same expansion rate Θ_i and thus the same

volume (cf. (9)). Consequently, $H_{\mathcal{D}} \rightarrow H_{\Lambda\text{CDM}}$ and $\Omega_k^{\mathcal{D}} \rightarrow -k/\dot{a}^2$. Therefore if $k = 0$ then also $\Omega_k^{\mathcal{D}} = 0$. Within the regime of linear perturbations, all quantities can be expressed in terms of density perturbations $\Delta\rho$. Since the average of linear perturbations vanishes, thus the average expansion coincides with the background expansion rate, i.e. $H_{\mathcal{D}} = H_{\Lambda\text{CDM}}$. Similarly, the average spatial curvature, within the linear regime is flat $\Omega_k^{\mathcal{D}} = 0$. It is only in the nonlinear regime when the spatial curvature emerges and the expansion rate increases compared to the Λ CDM model. This is presented in Fig. 1 where in the nonlinear regime ($t > 1$ Gyr) both spatial curvature and the expansion rate deviate from the Λ CDM model. It is interesting to note that in the dark energy dominated epoch ($t > 10$ Gyr) both the spatial curvature and expansion rate do asymptotically approach the Λ CDM model; this phenomenon is known as the “cosmic no-hair” conjecture [25].

However, it needs to be stressed that the expansion rate $H_{\mathcal{D}}$ (presented in Fig. 1) is not the same as the Hubble constant inferred from the distance ladder H_0^{DL} — it is only in the FLRW limit where the expansion rate and the slope of the distance-redshift relation are equivalent to each other [26]. Therefore, in order to estimate the Hubble parameter based on the distance ladder H_0^{DL} one needs to implement the ray-tracing method to the *Simsilun* simulation, which is described in the next section.

IV. LIGHT PROPAGATION

A. Distance and redshift

Apart from the evolution of the universe the ray-tracing is implemented within the *Simsilun* simulation. The light propagation is based on the Sachs optical equations [27]. The angular diameter distance D_A follows from

$$\frac{d^2 D_A}{ds^2} = -\left(\sigma^2 + \frac{1}{2} R_{ab} k^a k^b\right) D_A, \quad (17)$$

where σ is the shear of the null bundle k^a , and s is the affine parameter. The redshift follows from

$$\frac{dz}{ds} = \left(\frac{1}{3}\Theta + \Sigma_{ab} n^a n^b\right) (1+z)^2, \quad (18)$$

where Σ_{ab} the shear of the matter field and n^a is a unit vector in the direction of propagation. For comoving dust $R_{ab} k^a k^b = \rho(1+z)^2$ and for non-extreme cases (strong lensing) the null shear does not affect the distance-redshift relation [28]. Additionally, since there is no prefer direction, the average contribution from matter shear to the distance relation vanishes, as it only contributes via the trace [29].

Solving the above equations within the Simsilun simulation we find the relation between the angular diameter distance and redshift. Then using the reciprocity theorem [17] the luminosity distance is

$$D_L = (1+z)^2 D_A. \quad (19)$$

B. Generating the mock catalogues

In Ref. [2] the Hubble constant estimated based on low-redshift data was inferred using a two-stage analysis. First, the parameter a of eq. (4) was inferred from 217 supernova Ia with redshifts $0.0233 < z < 0.15$. Then various anchors were used to perform a simultaneous fit of supernova and Cepheid data to infer M , which in turn via (3) constrained the Hubble constant H_0^{DL} .

Within the Simsilun simulation the implemented ray-tracing algorithm provides the distances, consequently the last step of the calibration of M for the Simsilun simulation is not needed and the Hubble parameter H_0^{DL} can be estimated from

$$\log_{10} H_0^{\text{DL}} = \log_{10} \left(cz \left\{ 1 + \frac{1}{2} [1 - q_0] z - \frac{1}{6} [1 - q_0 - 3q_0^2 + j_0] z^2 \right\} \right) - \log_{10} D_L, \quad (20)$$

or in terms of the distance modulus from

$$\log_{10} H_0^{\text{DL}} = \log_{10} \left(cz \left\{ 1 + \frac{1}{2} [1 - q_0] z - \frac{1}{6} [1 - q_0 - 3q_0^2 + j_0] z^2 \right\} \right) - 0.2\mu + 5. \quad (21)$$

where the distance modulus is $\mu = 5 \log_{10} D_L + 25$.

To estimate the Hubble constant H_0^{DL} within the Simsilun simulation we generate 217 light rays with redshift $0.0233 < z_{0,i} < 0.15$, and calculate the luminosity distance $D_{0,i}$. To apply some realistic uncertainties we use the Union2.1 set [30]. We take uncertainties and covariance matrix from the Union2.1 dataset [51] for 217 supernova with $z < 0.2$ (Union2.1 consists of 580 supernova with redshift up to $z = 1.414$) and apply them to the Simsilun simulation distances. While this procedure is not ideal, it does provide ‘realistic’ uncertainties, that can be applied to the ‘ideal’ data generated using the Simsilun simulation. First, the uncertainty in the distance modulus is transform to uncertainty in each distance $D_{0,i}$

$$\Delta D_i = 0.2 \Delta \mu_i D_{0,i} \log_{10} 10,$$

and then the distances are Gaussian scattered

$$D_{L,i} = \mathcal{N}(\mu = D_{0,i}, \sigma = \Delta D_i),$$

where $\mathcal{N}(\mu = D_{0,i}, \sigma = \Delta D_i)$ is a random number drawn from a Gaussian distribution whose mean value is $D_{0,i}$ and standard deviation equal to distance uncertainty ΔD_i . Once the mock catalogue is generated, we

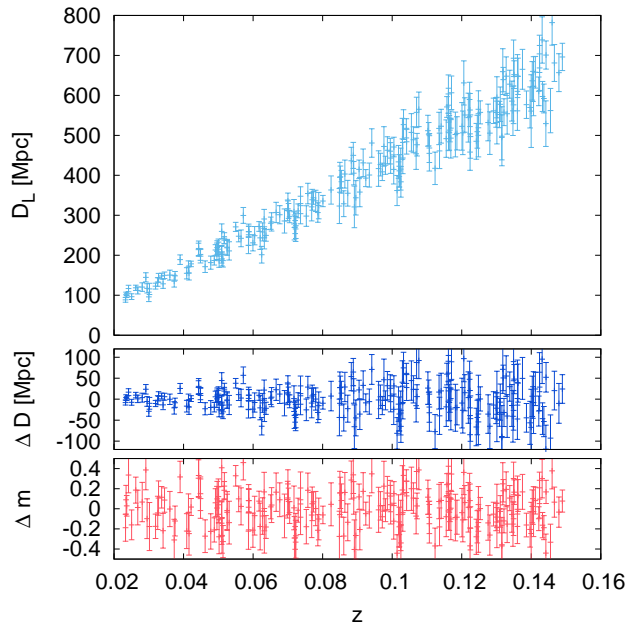


FIG. 2: A single mock supernova catalogue generated within the Simsilun simulation. 217 generated distance-redshift relations has been Gaussian scattered using uncertainties from the Union2.1 data set. Upper panel shows the luminosity distance D_L ; Middle panel shows distance residuals ΔD_L from the best-fit distance-redshift relation (1); Lower panel shows residuals in brightness $\Delta \mu = 5 \log_{10}(1 + \Delta D_L/D_L)$.

perform the MCMC analysis. The likelihood at each step is evaluated based on eq. (21) with the covariance matrix taken from the Union2.1 set. The MCMC analysis allows to estimate the mean, as well as, uncertainties in H_0^{DL} while treating the parameters q_0 and j_0 as the nuisance parameters. An example of a single mock catalogue (next sections considers multiple mocks) together with the residuals from the best-fit are presented in Fig. 2.

V. RESULTS

The results for the Hubble constant H_0^{DL} estimated using eq. (21) based on the ray-tracing within the Simsilun simulation are presented in Fig. 3. The results include the cosmic variance which was estimated using 10,000 mock catalogues with random observers. The Hubble constant is $H_0^{\text{DL}} = 72.5 \pm 2.1 \text{ km s}^{-1} \text{ Mpc}^{-1}$ and its pdf is presented with a red solid line in Fig. 3. It should be noted that the initial conditions for the Simsilun simulation were set up using the Planck data. When the Simsilun simulation was re-run with no inhomogeneities imposed, the Hubble constant inferred within such a homogeneous simulation [52] (using the mock catalogues

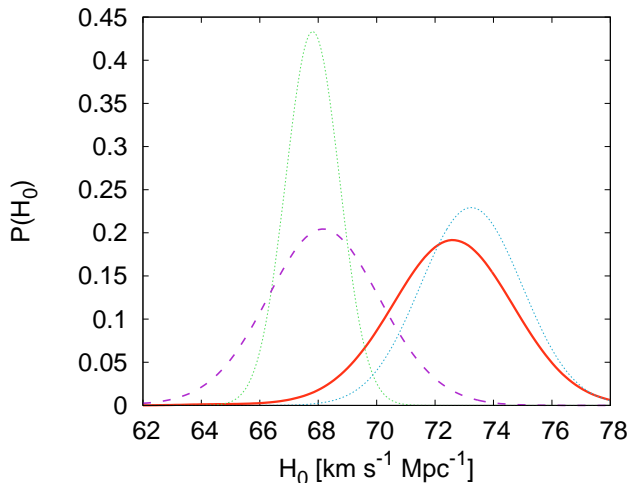


FIG. 3: The Hubble constant evaluated within the Simsilun simulation (red solid line). The constraints are inferred from the slope of the distance-redshift relation (21) and result with $H_0^{\text{DL}} = 72.5 \pm 2.1 \text{ km s}^{-1} \text{ Mpc}^{-1}$. If the Simsilun simulation is run with no inhomogeneities imposed (i.e. the FLRW case) then the Hubble constant inferred from the slope of the distance-redshift is $H_0^{\text{DL}} = 68.1 \pm 2.0 \text{ km s}^{-1} \text{ Mpc}^{-1}$ (purple dashed line). For comparison, the green dotted line (on the left) presents the Gaussian profile with the mean 67.81 and the standard deviation 0.92 (cf. CMB constraints [3]) and the blue dotted line (on the right) shows a Gaussian profile with the mean 73.24 $\text{km s}^{-1} \text{ Mpc}^{-1}$ and the standard deviation 1.74 $\text{km s}^{-1} \text{ Mpc}^{-1}$ (cf. distance ladder constraints [2]).

generated as described in Sec. IV B) was found to be $H_0^{\text{DL}} = 68.1 \pm 2.0 \text{ km s}^{-1} \text{ Mpc}^{-1}$. The pdf of the Hubble constant inferred from a homogeneous Simsilun simulation is presented with a purple dashed line in Fig. 3. This shows that relativistic non-linear evolution of a cosmic system, which allows for the emergence of the spatial curvature can solve the problem of the tension between high-redshift (CMB) and low-redshift (distance ladder) measurements of H_0 . For comparison the pdfs of these two measurements are presented in Fig. 3 using dotted lines [53].

VI. DISCUSSION ON THE ORIGIN OF THE EFFECT

The reason why the Simsilun simulation predicts a higher expansion rate has been partially explained in Sec. III B. However, there is an additional subtlety that needs to be discussed in regards to the results obtained in Sec. V.

The expansion rate of space follows from eq. (6). As seen from eq. (6), in the linear regime the only factor that causes the departure from the background's expansion rate Θ is the fluctuation in the density field $\rho = \bar{\rho} + \Delta\rho$.

Since the global average of density fluctuations vanishes, i.e. $\int dV \Delta\rho = 0$, a faster expansion rate of voids (where $\Delta\rho < 0$) is compensated by a slower expansion rate of overdense regions (where $\Delta\rho > 0$), consequently the average expansion rate coincides with the background's expansion rate.

Once the evolution becomes nonlinear, the symmetry between underdense and overdense regions starts to break. On the one side, as the underdense regions become emptier they expand faster; on the other side, the build-up of the shear Σ^2 within overdense regions slows down their expansion rate more efficiently than just the density perturbations alone. Consequently, the average expansion rate is faster compared to the ΛCDM model, i.e. $H_{\mathcal{D}} > (\dot{a}/a)_{\Lambda\text{CDM}}$.

For comparison, this effect is not present within the standard N-body simulations. Within the N-body simulations, matter is inhomogeneously distributed and even though one could map these fluctuations onto the shear and Weyl curvature, these quantities do not affect the overall expansion rate of the universe. Within the standard N-body simulations the expansion rate is given by eq. (12) and it is uniform everywhere, i.e. $H_0 = (\dot{a}/a)_{\Lambda\text{CDM}}$.

Within the Simsilun simulation cosmic voids occupy more volume than other regions, as a result if one picks a random line of sight, then along such a line of sight light most likely propagates through underdense regions. Although it sounds similar, this is not the Dyer-Roeder effect [31, 32], which is related to pure density fluctuations [33]. Here the effect is related to propagation through regions that expand faster than the background [34, 35]. Most importantly though, the effect reported in Sec. V should not be mistaken and contributed to ‘insufficient randomisation’ of the line of sights [36, 37]. On the contrary, had the insufficient randomisation been the issue, i.e. had we chosen light rays that propagate only through underdense regions then H_0^{DL} would have been up to 30% higher (instead of 6.5% higher) compared to the ΛCDM model. The fact that the Hubble constant inferred from the distance-redshift relation H_0^{DL} is so similar to the average expansion rate of space $H_{\mathcal{D}}$ empirically confirms results obtained in Refs. [28, 38, 39], which suggest that the average distance-redshift relation should follow the average expansion rate.

As seen from Fig. 1, once the evolution becomes nonlinear, the average expansion rate starts to deviate from the background's ΛCDM model, thus the present-day expansion rate inferred from the distance-redshift relation should be higher than the Hubble constant inferred from the conditions of the early universe, i.e. $H_0^{\text{DL}} > H_0^{\text{CMB}}$. This expectation is indeed confirmed by the results presented in Fig. 3.

VII. CONCLUSIONS

The history of measurements of the Hubble constant shows how its value, at various stages of time, was susceptible to number of observational biases. During the 20th century the value of the Hubble constant was subject to number of changes: misclassification of Cepheids, confusion between stars and HII regions, and especially the Malmquist bias [40] often led to overestimation of its value. However, when at the turn of the century the HST Key Project settled its value to $72 \pm 8 \text{ km s}^{-1} \text{ Mpc}^{-1}$ [41] it seemed that most systematics got under control. Yet when 10 years later, the 7-year WMAP data pointed towards $H_0^{\text{CMB}} = 70.2 \pm 1.4 \text{ km s}^{-1} \text{ Mpc}^{-1}$ [42] and the distance ladder method towards $H_0^{\text{DL}} = 73.8 \pm 2.4 \text{ km s}^{-1} \text{ Mpc}^{-1}$ [43], the debate on the Hubble constant got revived. The tension between high-redshift measurements (CMB) and low-redshift (distance ladder) got further widen with the Planck measurements, which constrained it to $H_0^{\text{CMB}} = 67.3 \pm 1.2 \text{ km s}^{-1} \text{ Mpc}^{-1}$ [44]. The inconsistency between these measurements seems to be statistically significant and does not seem to appear simply because we have two different types of measurements [45]. This suggest there must be some mechanism behind this inconsistency, be it either unaccounted systematics or some physical phenomenon.

The issue of systematics in the distance ladder method resurfaced when it was pointed out that various assumptions regarding the calibrations can shift the value of the Hubble constant by $2 \text{ km s}^{-1} \text{ Mpc}^{-1}$ [46]. Given the lack of compelling evidence for ‘new physics’ [47] it seemed likely that once again (as often in the past) the systematics were to be blamed for overestimating the Hubble constant. However, a careful analysis of the distance ladder using multiple anchors resulted with $H_0^{\text{DL}} = 73.24 \pm 1.74 \text{ km s}^{-1} \text{ Mpc}^{-1}$ [2], which confirmed the tension. The tension was further solidified with the latest Planck measurements, which set the high-redshift Hubble constant to $H_0^{\text{CMB}} = 67.81 \pm 0.92 \text{ km s}^{-1} \text{ Mpc}^{-1}$ [3].

This paper explored an extension of the Λ CDM model. This extension does not require any new physics in terms of the dark sector (e.g. evolving dark energy or interacting dark matter) or in terms of modification of gravity. The solution that this paper provides is more prosaic. It relies on the fact that the Einstein equations are nonlinear and therefore the evolution of an inhomogeneous nonlinear system that only in a statistical sense is homogeneous and isotropic (i.e. after averaging over sufficiently large domains) is not exactly the same as the evolution of an exactly homogeneous and isotropic system [5].

This paper uses the Sinsilun simulation that solves the Einstein equations within the approximation of the Silent Universes [15]. Within the framework of the Sinsilun simulation the spatial curvature evolves from spatial flatness of the early universe to a slightly negative values at the present day. A slight increase of the spatial curvature speeds up the expansion rate, which is presented in Fig. 1. The implementation of the ray-tracing algorithm

within the Sinsilun simulation allowed to generate mock supernova data, which were used to estimate the low-redshift Hubble constant H_0^{DL} directly from the distance-redshift relation. The initial conditions for the Sinsilun simulation has been setup in the early universe around the Planck’s Λ CDM model [3]. 10,000 mock catalogues has been generated (an example of a mock catalogue with uncertainties imposed from Union2.1 set [30] is presented in Fig. 2). The analysis showed that the phenomenon of emergence of the spatial curvature can solve the Hubble constant problem. As shown in Fig. 3, if the evolution of the universe follows exactly the equation of a purely homogeneous and isotropic universe (FLRW case) then the tension between the low-redshift and high-redshift Hubble constant appears. If however, relativistic corrections due to nonlinear cosmic evolution are included, then the tension is alleviated. The results of the evolution and ray-tracing algorithms within the Sinsilun simulation show that starting from the initial conditions as prescribed by the Planck satellite ($\omega_m = \Omega_m h^2 = 0.1415$, and $\omega_\Lambda = \Omega_\Lambda h^2 = 0.3182$ [3]) the present-day expansion rate should in fact be $H_0 = 72.5 \pm 2.1 \text{ km s}^{-1} \text{ Mpc}^{-1}$, which is in agreement with the low-redshift distance ladder measurements of $H_0^{\text{DL}} = 73.24 \pm 1.74 \text{ km s}^{-1} \text{ Mpc}^{-1}$ [2].

While these results are encouraging, it needs to be noted that the Sinsilun simulation is not a fully relativistic simulation of our Universe, but it relies on the approximation of the Silent Universe [15]. Other approaches and approximations to the relativistic numerical cosmology, such as the one based on the weak-field limit do not show the phenomenon of emerging spatial curvature [14] and therefore do not provide the solution of the Hubble constant problem. At this stage, the phenomenon of the emerging spatial curvature does seem to be a viable and attractive explanation of the Hubble constant problem. In fact, one can turn the argument around and argue that the presence of the tension between low and high-redshift measurements is a moderate (indirect) evidence for the phenomenon of emerging spatial curvature. From the point of view of astronomical observations, we still do not have a direct measurement of the spatial curvature at low-redshifts. Currently, the low-redshift measurements do not provide any direct measurement of the spatial curvature (available constrains merely result from fitting the FLRW geometry to the data, which is not equivalent to a direct measurement). The situation will change in a few years time with the data from the satellite Euclid [8, 48].

In summary, the results presented in this paper show that the phenomenon of emerging spatial curvature can provide the solution the Hubble constant problem and alleviate the tension between the low and high-redshift measurements, but it will take a few more years of theoretical and observational work before we will be able to confirm with full certainty that this phenomenon does in fact occur in our Universe.

Acknowledgements

This work was supported by the Australian Research Council through the Future Fellowship FT140101270. The Millennium simulation databases used in this paper and the web application providing online access to them

were constructed as part of the activities of the German Astrophysical Virtual Observatory (GAVO). Computational resources used in this work were provided by the ARC (via FT140101270) and the University of Sydney HPC service (Artemis).

-
- [1] T. Buchert, A. A. Coley, H. Kleinert, B. F. Roukema, and D. L. Wiltshire, *Int. J. Mod. Phys. D* **25**, 1630007-244 (2016), 1512.03313.
- [2] A. G. Riess, L. M. Macri, S. L. Hoffmann, D. Scolnic, S. Casertano, A. V. Filippenko, B. E. Tucker, M. J. Reid, D. O. Jones, J. M. Silverman, et al., *Astroph. J.* **826**, 56 (2016), 1604.01424.
- [3] Planck Collaboration, P. A. R. Ade, N. Aghanim, M. Arnaud, M. Ashdown, J. Aumont, C. Baccigalupi, A. J. Banday, R. B. Barreiro, J. G. Bartlett, et al., *Astron. Astrophys.* **594**, A13 (2016), 1502.01589.
- [4] A. H. Guth, *Phys. Rev. D* **23**, 347 (1981).
- [5] T. Buchert, M. Carfora, G. F. R. Ellis, E. W. Kolb, M. A. H. MacCallum, J. J. Ostrowski, S. Räsänen, B. F. Roukema, L. Andersson, A. A. Coley, et al., *Class. Quant. Grav.* **32**, 215021 (2015), 1505.07800.
- [6] T. Buchert and M. Carfora, *Classical and Quantum Gravity* **25**, 195001 (2008), 0803.1401.
- [7] X. Roy, T. Buchert, S. Carloni, and N. Obadia, *Classical and Quantum Gravity* **28**, 165004 (2011), 1103.1146.
- [8] S. Räsänen, K. Bolejko, and A. Finoguenov, *Phys. Rev. Lett.* **115**, 101301 (2015), 1412.4976.
- [9] K. Bolejko and M. Korzyński, *International Journal of Modern Physics D* **26**, 1730011 (2017), 1612.08222.
- [10] F. Löffler, J. Faber, E. Bentivegna, T. Bode, P. Diener, R. Haas, I. Hinder, B. C. Mundim, C. D. Ott, E. Schnetter, et al., *Classical and Quantum Gravity* **29**, 115001 (2012), 1111.3344.
- [11] E. Bentivegna and M. Bruni, *Phys. Rev. Lett.* **116**, 251302 (2016), 1511.05124.
- [12] J. B. Mertens, J. T. Giblin, and G. D. Starkman, *Phys. Rev. D* **93**, 124059 (2016), 1511.01106.
- [13] H. J. Macpherson, P. D. Lasky, and D. J. Price, *Phys. Rev. D* **95**, 064028 (2017), 1611.05447.
- [14] J. Adamek, C. Clarkson, D. Daverio, R. Durrer, and M. Kunz, *ArXiv e-prints* (2017), 1706.09309.
- [15] K. Bolejko, *Classical and Quantum Gravity* **35**, 024003 (2018), 1708.09143.
- [16] G. Hinshaw, D. Larson, E. Komatsu, D. N. Spergel, C. L. Bennett, J. Dunkley, M. R.olta, M. Halpern, R. S. Hill, N. Odegard, et al., *Astroph. J. Supp.* **208**, 19 (2013), 1212.5226.
- [17] G. F. R. Ellis, in *General Relativity and Cosmology*, edited by R. K. Sachs (1971), pp. 104–182.
- [18] G. F. R. Ellis, *General Relativity and Gravitation* **41**, 581 (2009).
- [19] M. Bruni, S. Matarrese, and O. Pantano, *Astroph. J.* **445**, 958 (1995), astro-ph/9406068.
- [20] H. van Elst, C. Ugglá, W. M. Lesame, G. F. R. Ellis, and R. Maartens, *Classical and Quantum Gravity* **14**, 1151 (1997), gr-qc/9611002.
- [21] R. Maartens, W. M. Lesame, and G. F. R. Ellis, *Phys. Rev. D* **55**, 5219 (1997), gr-qc/9703080.
- [22] V. Springel, S. D. M. White, A. Jenkins, C. S. Frenk, N. Yoshida, L. Gao, J. Navarro, R. Thacker, D. Croton, J. Helly, et al., *Nature* **435**, 629 (2005), astro-ph/0504097.
- [23] M. Boylan-Kolchin, V. Springel, S. D. M. White, A. Jenkins, and G. Lemson, *Mon. Not. R. Astron. Soc.* **398**, 1150 (2009), 0903.3041.
- [24] Q. Guo, S. White, R. E. Angulo, B. Henriques, G. Lemson, M. Boylan-Kolchin, P. Thomas, and C. Short, *Mon. Not. R. Astron. Soc.* **428**, 1351 (2013), 1206.0052.
- [25] K. Bolejko, *Phys. Rev. D* **97** (2018).
- [26] A. Krasinski, C. Hellaby, K. Bolejko, and M.-N. Célérier, *Gen. Rel. Grav.* **42**, 2453 (2010), 0903.4070.
- [27] R. Sachs, *Proceedings of the Royal Society of London Series A* **264**, 309 (1961).
- [28] K. Bolejko and P. G. Ferreira, *J. Cosmol. Astropart. Phys.* **5**, 003 (2012), 1204.0909.
- [29] S. Räsänen, *J. Cosmol. Astropart. Phys.* **3**, 018 (2010), 0912.3370.
- [30] N. Suzuki, D. Rubin, C. Lidman, G. Aldering, R. Amanullah, K. Barbary, L. F. Barrientos, J. Botyanszki, M. Brodwin, N. Connolly, et al., *Astroph. J.* **746**, 85 (2012), 1105.3470.
- [31] C. C. Dyer and R. C. Roeder, *Astroph. J.* **174**, L115 (1972).
- [32] C. C. Dyer and R. C. Roeder, *Astroph. J.* **180**, L31 (1973).
- [33] K. Bolejko, *Mon. Not. R. Astron. Soc.* **412**, 1937 (2011), 1011.3876.
- [34] C. Clarkson, G. F. R. Ellis, A. Faltenbacher, R. Maartens, O. Umeh, and J.-P. Uzan, *Mon. Not. R. Astron. Soc.* **426**, 1121 (2012), 1109.2484.
- [35] N. Meures and M. Bruni, *Mon. Not. R. Astron. Soc.* **419**, 1937 (2012), 1107.4433.
- [36] R. A. Vanderveld, É. É. Flanagan, and I. Wasserman, *Phys. Rev. D* **78**, 083511 (2008), 0808.1080.
- [37] K. Kainulainen and V. Marra, *Phys. Rev. D* **80**, 123020 (2009), 0909.0822.
- [38] S. Räsänen, *J. Cosmol. Astropart. Phys.* **2**, 011 (2009), 0812.2872.
- [39] N. Kaiser and J. A. Peacock, *Mon. Not. R. Astron. Soc.* **455**, 4518 (2016), 1503.08506.
- [40] G. A. Tammann, in *Reviews in Modern Astronomy*, edited by S. Roeser (2006), vol. 19 of *Reviews in Modern Astronomy*, p. 1, astro-ph/0512584.
- [41] W. L. Freedman, B. F. Madore, B. K. Gibson, L. Ferrarese, D. D. Kelson, S. Sakai, J. R. Mould, R. C. Kennicutt, Jr., H. C. Ford, J. A. Graham, et al., *Astroph. J.* **553**, 47 (2001), astro-ph/0012376.
- [42] E. Komatsu, K. M. Smith, J. Dunkley, C. L. Bennett, B. Gold, G. Hinshaw, N. Jarosik, D. Larson, M. R.olta, L. Page, et al., *Astroph. J. Supp.* **192**, 18 (2011), 1001.4538.

- [43] A. G. Riess, L. Macri, S. Casertano, H. Lampeitl, H. C. Ferguson, A. V. Filippenko, S. W. Jha, W. Li, and R. Chornock, *Astroph. J.* **730**, 119 (2011), 1103.2976.
- [44] Planck Collaboration, P. A. R. Ade, N. Aghanim, C. Armitage-Caplan, M. Arnaud, M. Ashdown, F. Atrio-Barandela, J. Aumont, C. Baccigalupi, A. J. Banday, et al., *Astron. Astrophys.* **571**, A16 (2014), 1303.5076.
- [45] W. Lin and M. Ishak, *Phys. Rev. D* **96**, 083532 (2017), 1708.09813.
- [46] G. Efstathiou, *Mon. Not. R. Astron. Soc.* **440**, 1138 (2014), 1311.3461.
- [47] C. L. Bennett, D. Larson, J. L. Weiland, and G. Hinshaw, *Astroph. J.* **794**, 135 (2014), 1406.1718.
- [48] K. Bolejko, ArXiv e-prints (2017), 1707.01800.
- [49] <https://bitbucket.org/bolejko/simsilun>
- [50] The MField database is accessible via the German Astrophysical Virtual Observatory <http://gavo.mpa-garching.mpg.de/MyMillennium> with the SQL query `select * from MField..MField`.
- [51] The supernova data as well as the covariance matrix for the Union2.1 set is accessible via the website of the Supernova Cosmology Project <http://supernova.lbl.gov/Union/>.
- [52] A homogeneous Simsilun simulation is the one where the initial density contrast vanish everywhere $\delta_i = 0$, this means that $\Sigma = 0$ and $\mathcal{W} = 0$ and so the system is equivalent to the FLRW system (cf. Sec. III A 1), however the evolution is still traced by solving eqs. (5)–(9).
- [53] To be precision, the dotted lines shows Gaussian profiles: one with the mean $\mu = 67.81$ and standard deviation $\sigma = 0.92$ (CMB), and the other one with $\mu = 73.24$ and $\sigma = 1.74$ (distance ladder).